PHYSICS AND CHEMISTRY OF SOLID STATE
V. 22, No. 4 (2021) pp. 697-710
Section: Chemistry

DOI: 10.15330/pcss.22.4.697-710

Vasyl Stefanyk Precarpathian National University

ФІЗИКА І ХІМІЯ ТВЕРДОГО ТІЛА
Т. 22, № 4 (2021) С. 697-710
Хімічні науки

UDC 544.47

ISSN 1729-4428

Ivan Mironyuk, Nazarii Danyliuk, Tetiana Tatarchuk, Ihor Mykytyn, Volodymyr Kotsyubynsky

Photocatalytic degradation of Congo red dye using Fe-doped TiO_2 nanocatalysts

Vasyl Stefanyk Precarpathian National University, Ivano-Frankivsk, Ukraine, e-mail: danyliuk.nazariy@gmail.com

Fe-doped TiO_2 (2, 5, 10, 15 and 20% wt. of Fe) photocatalysts have been synthesized by sol-gel method using titanium aquacomplex precursor. The structure and morphology have been characterized by XRD, BET, SEM, and EDS analyses, Mossbauer and IR spectroscopies. XRD analysis confirmed the anatase structure. The introduction of ferric ions into the titania structure causes its amorphization. The crystallite sizes of obtained samples are around 3 nm. Fe-doped TiO_2 samples possess mesoporous structure and high specific surface area (from 274 m^2g^{-1} for 5Fe-TiO_2 to 416.4 m^2g^{-1} for 20Fe-TiO_2). Mossbauer spectroscopy data confirms the incorporation of Fe^{3+} ions in the anatase structure. Photocatalytic degradation of Congo red dye using Fe-doped TiO_2 photocatalysts was studied under the UV-A light. Optimized conditions for photocatalytic degradation of CR in the presence of hydrogen peroxide are obtained. It was found that the 2Fe-TiO_2 sample in the presence of 20 mM H_2O_2 solution showed highest efficiency in dye photodegradation (99.4%) under UV-A light. The photodegradation kinetics was analyzed using a smartphone and fits well with first-order kinetics model.

Keywords: Fe-doped TiO_2; Photocatalysis; Congo red; Smartphone.

Received 21 September 2021; Accepted 11 November 2021.

Introduction

The anionic and cationic dyes are the main pollutants of the wastewater derived from textile enterprises. As a rule, dyes contain extremely dangerous, carcinogenic components (benzene rings, sulfonate and amino groups) which can cause considerable harm to human health and the environment [1]. Even at very low concentrations (<1 ppm) the organic dyes significantly worsen the state of the aquatic environment [2–4]. There are many technologies for pre-treatment of wastewater from the textile industry, but they are inefficient. The common methods of dyes removal from aqueous medium are adsorption [5] and coagulation [6], but the main disadvantage of those methods is that the dye is removed from the solution by a non-destructive method and its structure remains intact. Instead, a heterogeneous photocatalysis is a promising technology that causes the more efficient and non-selective dyes destruction in aqueous systems [7–12]. However, its practical application has several limitations: i) a low quantum efficiency; ii) the difficultness in photocatalyst obtaining; iii) the dependence on ultraviolet (UV) light source. However, despite all these limitations, photocatalysis demonstrates many advantages over traditional wastewater treatment methods. The main one is that organic pollutants can be completely mineralized to CO_2 and H_2O without the formation of secondary hazardous products [13,14]. It is known that the process of photodegradation is influenced by the following parameters such as photocatalyst morphology [15], solution pH [16], initial dye concentration [17], reaction temperature [18], H_2O_2 impact [19] and the light intensity [20]. In particular, the impact of different physical properties (particles size and shape, surface area, crystal structure and phase composition) on the

photocatalytic properties of nano-TiO_2 was studied by R.K. Wahi et al. [15]. Photodecomposition experiments indicated that anatase is a more active photocatalyst compared to rutile.

Recently, many researchers have reported the enhanced photocatalytic and adsorption properties as a result of TiO_2 modifications by noble metals doping [21], transition metals doping [22–25], and surface modification by anions [26–28]. For example, Alamelu et al. [29] investigated a composite photocatalyst TiO_2-Pt for efficient removal of 4-nitrophenol and Rhodamine B from an aqueous medium using chemical reduction and photocatalytic degradation, respectively. Synthesis of TiO_2-Pt catalysts with different Pt amount (from 1 to 10%), carried out by hydrothermal method, followed by chemical reduction. As a result, it was found that Pt leads to an increase in catalytic properties. The best results were obtained for the composite with 5 wt.% of Pt, which showed a 4.5-fold increase in photocatalytic destruction of RhB and a 45-fold increase in the reduction of 4-nitrophenol (4-NP) compared with unsubstituted TiO_2. In addition, this photocatalyst showed high stability when tested on five consecutive cycles of photodegradation. The authors explain the enhanced photoactivity of TiO_2-Pt catalysts by its strong adsorption capacity regarding to RhB and 4-NP, large surface area and increased electron transfer provided by Pt NPs. Anwar et al. [30] synthesized the Fe-TiO_2 composite (with an Fe content of 6% wt.) by the sol-gel method, followed by heat treatment at 500℃, for the photodestruction of Methylene blue dye under visible light. As a result, the degradation of Methylene blue was 36% without irradiation (at pH = 10) and 99.5% under visible light irradiation for 3 hours. Asiltürk et al. [31] investigated the impact of Fe^{3+} doping on the photocatalytic activity of TiO_2 coated glass under the influence of UV and visible light. The Malachite green (MG) dye has been used as model pollutant. The study found that the degradation efficiency of Fe-doped TiO_2 coated glass surfaces was higher than the pure TiO_2 coated surface. It was concluded that the MG photodestruction (2.5 mg/L) by Fe-doped TiO_2 under UV light refers to the pseudo-first order kinetics with a rate constant k=0.0202 min^{-1}.

Congo red (CR) is widely used as a model substance to study the efficiency of azo dyes degradation using TiO_2 [7,15]. For example, Wahab et al. [7] showed that complete CR discoloration was achieved in 3 hours using 2.5%N-TiO_2 and visible light as radiation source. Arora et al. [8] investigated the efficiency of Cu-loaded Fe_3O_4@TiO_2 composite as photocatalyst for CR degradation using 15W UV lamp (350–400 nm). Thus, the aim of this study is to synthesize Fe-doped TiO_2, which would quickly decompose the CR dye under UV-A light. The hydrogen peroxide (H_2O_2) is used as external electron acceptor. Recently, only a few attempts have been made to use Fe-doped TiO_2 photocatalyst with enhanced activity for the azo dyes decomposition [32–35]. Therefore, this concept is a relevant topic for further research. In this work, Fe-doped TiO_2 photocatalysts were synthesized using a modified sol-gel method. The degradation conditions were optimized to achieve the best photocatalyst efficiency. The photocatalytic activity of the synthesized Fe-doped TiO_2 was compared with the efficiency of commercial P25-TiO_2.

I. Materials and methods

1.1. Materials

Congo Red dye (CR) was obtained from Sigma-Aldrich, used without further purification. Titanium chloride $TiCl_4$ (99.9%, Merck). Concentrated chloric acid (1.190 g/cm^3). Ferric chloride hexahydrate (Merck, reagent grade, ≥98%). P25-TiO_2 (Evonik) contains 80% of anatase and 20% of rutile with a surface area of 50 m^2g^{-1} and an average particle size of 30 nm. Reagent grade hydrogen peroxide (31.5%) was obtained from SferaSim (Ukraine).

1.2. Synthesis of unmodified and modified titania photocatalyst

A titanium aquacomplex $[Ti(OH_2)_6]^{3+}\cdot 3Cl^-$ precursor was obtained according to [27] and [36]. Ferric chloride hexahydrate was added to the precursor solution to obtain Fe-doped TiO_2 (2, 5, 10, 15 and 20% wt.). The synthesis conditions for unmodified and modified titania are given in Table 1. The precursor solution with the modifying component was diluted with water. The NaOH solution has been added to maintain pH = 1…2. The mixture was kept at 70ºC for 30-40 minutes. At the end of the process, the mixture pH was adjusted to pH=6…7. The formed particles were removed from the reaction medium with a vacuum filter. They were washed from Na^+ and Cl^- ions with distilled water and dried at a temperature of 120-140ºC.

Table 1

Synthesis conditions for unmodified and modified titania (343 K)

Sample	Precursor	Modifier	Modifier content, wt.%	Duration, min
TiO_2	$[Ti(OH_2)_6]^{3+}\cdot 3Cl^-$	-	0	30-40
2Fe-TiO_2	$[Ti(OH_2)_6]^{3+}\cdot 3Cl^-$	Fe^{3+}	2	30-40
5Fe-TiO_2	$[Ti(OH_2)_6]^{3+}\cdot 3Cl^-$	Fe^{3+}	5	30-40
10Fe-TiO_2	$[Ti(OH_2)_6]^{3+}\cdot 3Cl^-$	Fe^{3+}	10	30-40
15Fe-TiO_2	$[Ti(OH_2)_6]^{3+}\cdot 3Cl^-$	Fe^{3+}	15	30-40
20Fe-TiO_2	$[Ti(OH_2)_6]^{3+}\cdot 3Cl^-$	Fe^{3+}	20	30-40

1.3. Characterization techniques

1.3.1. XRD

The phase composition of the photocatalyst was analysed by XRD method at $\lambda_{K\alpha 1}$ = 0.154 nm (STOE STADI P diffractometer, Germany). The average size of crystallites was calculated by Scherrer's formula:

$$< D >= \frac{0.9\lambda}{\beta_{(311)}\cos\theta},$$

where $\beta_{(311)}$ is the full width at half maximum of the (311) reflection, θ is Bragg angle of reflection.

1.3.2. N_2 adsorption

The pore size distribution of the Fe-doped TiO_2 sample was measured by the N_2 adsorption/desorption method using surface area analyzer Quantachrome Autosorb, Nova 2200e, at temperature 77 K.

1.3.3. SEM and EDS

The morphology of TiO_2 was investigated by scanning electron microscopy (SEM) with an attachment for energy dispersion analysis (REMMA-102-02 Scanning Electron Microscope-Analyzer (JCS SELMI, Ukraine)). The accelerating voltage was 20.00kV.

1.3.4. Mossbauer spectroscopy

Mössbauer spectra were measured with MS-1104Em spectrometer (^{57}Co(Cr) radioactive source, activity of about 40 mCi) at 90 K. Calibration of the isomer shifts was done respectively to α-Fe standard (line width 0.29 mm/s). The spectra analysis and fitting procedure were performed using UnivemMs 701 software.

1.3.5. IR spectroscopy

Infrared spectra of TiO_2 samples were registered on the SPECORD M80 spectrophotometer in the range of 4000-300 cm^{-1}. To record the spectrum, 4 mg of the sample was mixed with dry KBr in the ratio of 1:100 and crushed in a vibrating mill for 5 min. The prepared mixture was compressed to form transparent pellets (20×5 mm^2).

1.4. Photodegradation experiments

The photocatalytic micro-photoreactor consists of a glass vessel (volume 20 mL), a light source, magnetic stirrer and a movable cuvette holder. All photocatalytic experiments were performed at room temperature (25±2ºC). The light source was a 3W UV LED (365 nm) mounted on the outside of the photoreactor, which was located vertically relative to the reactor. Photocatalyst powders were completely dispersed in aqueous CR solution. A more detailed description is presented in our previous work [37]. Registration of photocatalysis kinetics was performed using a smartphone, the details of the measurements are described in [37]. The UV-Vis spectra were obtained in the range 340–750 nm using ULAB 102-UV spectrophotometer and 5 mm quartz cuvettes. Calibration line was plotted using absorbance at 500 nm versus CR dye concentration in the range from 0 to 50 mg/L.

II. Results and discussion

2.1. Synthesis of Fe-doped TiO_2 samples

The aim of this work was to synthesize titanium dioxide with Fe atoms, intercalated in its structure and to find out how the Fe intercalation affects the crystal structure and morphology of the oxide material and its photocatalytic activity. The solutions of aquacomplexes $[Ti(OH_2)_6]^{3+}\cdot 3Cl^-$ and $[Fe(OH_2)_6]^{2+}\cdot 2Cl^-$ used as precursors for obtaining oxide materials. A solution of titanium aquacomplex was obtained by mixing concentrated hydrochloric acid, cooled to a temperature (-5…-0) ℃ with titanium tetrachloride in a mass ratio of $TiCl_4$/HCl = 1.4/1.0. A solution of the aquacomplex precursor $[Fe(OH_2)_6]^{2+}\cdot 2Cl^-$ was obtained by mixing $FeCl_3$ with concentrated hydrochloric acid. The oxide materials Fe-TiO_2 contain 2; 5; 10; 15 and 20 wt.% of Fe. Precursors' solutions were mixed in the required ratio and kept for 30-40 minutes at a temperature of 70 ℃. Then a 4% NaOH solution was added dropwise to the cooled mixture, thus raising the pH of the reaction medium from 0.5 to 6.5…7.0. The formed Fe-TiO_2 particles were removed from the reaction medium, washed with deionized water from the Na and Cl ions and dried at a temperature of 110-130ºC. The formation of Fe-TiO_2 particles is carried out in two stages: during the heating of the mixture of precursors' solutions and during the NaOH adding. Approximately a third part of the oxide material is formed in the first stage, and the rest in the second stage. The first stage is occurs due to the spontaneous oxidation of Ti (III) and Fe (II) cations:

$$Ti\,(III) \rightarrow Ti\,(IV) + e^- \quad (1)$$

$$Fe\,(II) \rightarrow Fe\,(III) + e^- \quad (2)$$

The released electrons cause the reduction of water molecules located near the Ti(IV) and Fe (III) cations due to chemical reaction:

$$4H_2O + O_2 + 4e \rightarrow 4OH^- \quad (3)$$

The molecules of the absorbed oxygen take part in this reaction. The formed OH^- anions attach to metal cations. Since the electronegativity of Ti atoms is 1.5, the $Ti(OH)_3$ molecules are the first to be formed in the reaction medium. They dissociate into $[FeO_3]^{3-}$ anions and $3H^+$ cations. In turn, these anions join the titanium cations in their aquacomplexes:

$$[Ti(OH)(OH_2)_5]^{3+}\cdot 3Cl^- + [FeO_3]^{3-}\cdot 3H^+ \rightarrow [Ti(OH)(OH_2)_4OFe(OH)_2]^{2+}\cdot 2Cl^- + HCl + H_2O \quad (4)$$

The introduction of NaOH into the reaction medium causes that most of the precursors mixture is converted into $Ti(OH)_4$ and $Fe(OH)_3$ molecules, which due to the polycondensation process form a complex Fe-TiO_2 oxide.

2.2. Characterization

2.2.1. XRD

The diffractograms of Fe-doped TiO_2 samples shown in Fig. 1. They confirm that the samples of Fe-doped TiO_2 (2...20%) are single-phase. Their crystal structure belongs to the anatase structure (space group I41/amd). The structural parameters of the crystal lattice (*a* and *c*) of the synthesized Fe-doped TiO_2 samples are shown in Fig. 2. The introduction of Fe ions causes structure amorphization (Fig. 1). The crystallite sizes of anatase, calculated by the Scherrer equation from peak (101) do not change (mostly 3 nm). The crystallinity of TiO_2 decreases with Fe increasing and the sample with the maximum degree of Fe doping (20%) is amorphous. The formation of Fe_2O_3 phase does not observed. X-ray diffraction patterns of the samples with a high content of Fe (10; 15; and 20 wt.%) do not have peaks of Fe(III) oxide.

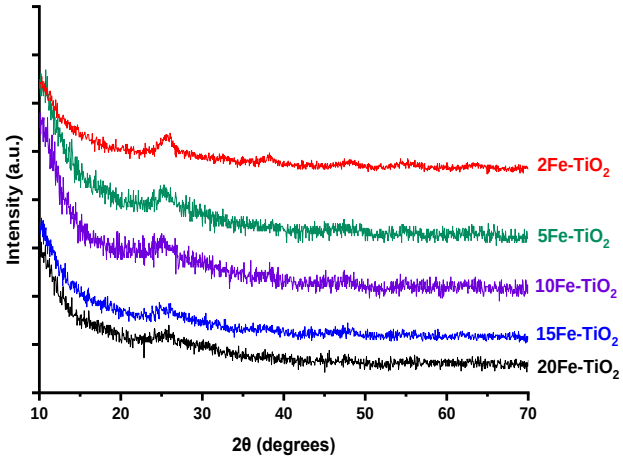

Fig. 1. XRD patterns of Fe-doped TiO2 samples

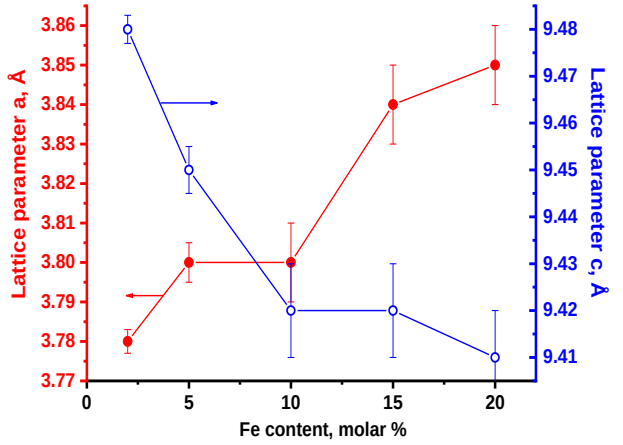

Fig. 2. The lattice constant of anatase phase as a function of iron content.

2.2.2. N_2 adsorption

Figure 3a shows the N_2 adsorption/desorption isotherms of Fe-doped TiO_2 samples obtained at 77K. The parameters of the photocatalyst porous structure are given in Table 2, and the pore size distribution is shown in Fig. 3b. The most micropores have a radius of ~2 nm and the radii of mesopores do not exceed 2.5 nm. The peak corresponds to pores with a radius of ~1.8 nm. The specific surface area of Fe-doped TiO_2 samples increases from 274 $m^2 \cdot g^{-1}$ (for 5Fe-TiO_2) to 416.4 $m^2 \cdot g^{-1}$ (for 20Fe-TiO_2) (Table 2).

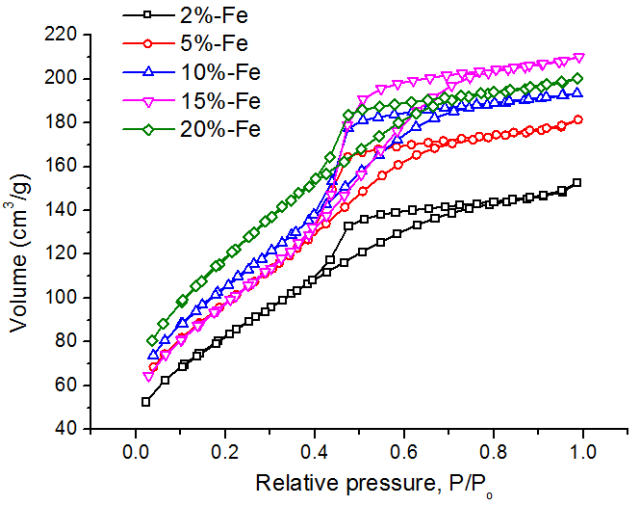

a)

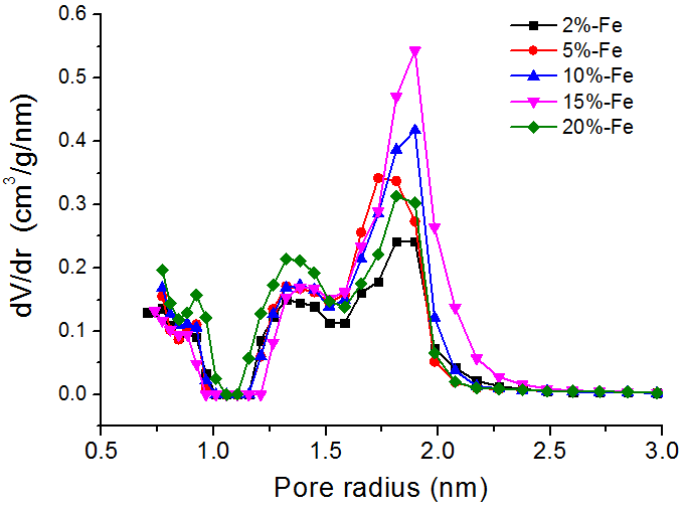

b)

Fig. 3. (a) N_2 adsorption/desorption isotherms and (b) pore size distribution of the Fe-doped TiO_2 samples.

2.2.3. SEM and EDS

SEM images showed particle size and morphology in approximate dimensions. Studies of synthesized Fe-doped TiO_2 samples found that the primary particles have a different shape (Fig. 4).

The results of the energy-dispersion analysis are shown in Fig. 5. They confirm the chemical composition of the synthesized Fe-doped TiO_2 samples. It is seen that only Ti, O and Fe elements are present in the samples. The obtained percentage of the elements is close to the stoichiometry (Fig. 5).

Table 2

Textural characteristics (specific surface area, pore volume)

Sample	S_{BET} (m^2g^{-1})	S_{micro} (m^2g^{-1})	S_{meso}, (m^2g^{-1})	V_{pore}, (cm^3g^{-1})	V_{micro} (cm^3g^{-1})	V_{meso} (cm^3g^{-1})	V_{meso}/V_p (%)
TiO_2	239.4	100.50	138.90	0.1519	0.054	0.098	64.5
2Fe-TiO_2	274.5	5.52	268.98	0.236	0.0137	0.2223	94.2
5Fe-TiO_2	347.6	-	347.6	0.2807	-	0.2807	100
10Fe-TiO_2	371.6	-	371.6	0.299	-	0.299	100
15Fe-TiO_2	351.7	-	351.7	0.325	-	0.325	100
20Fe-TiO_2	416.4	72.66	343.74	0.3097	0.039	0.2707	87.4

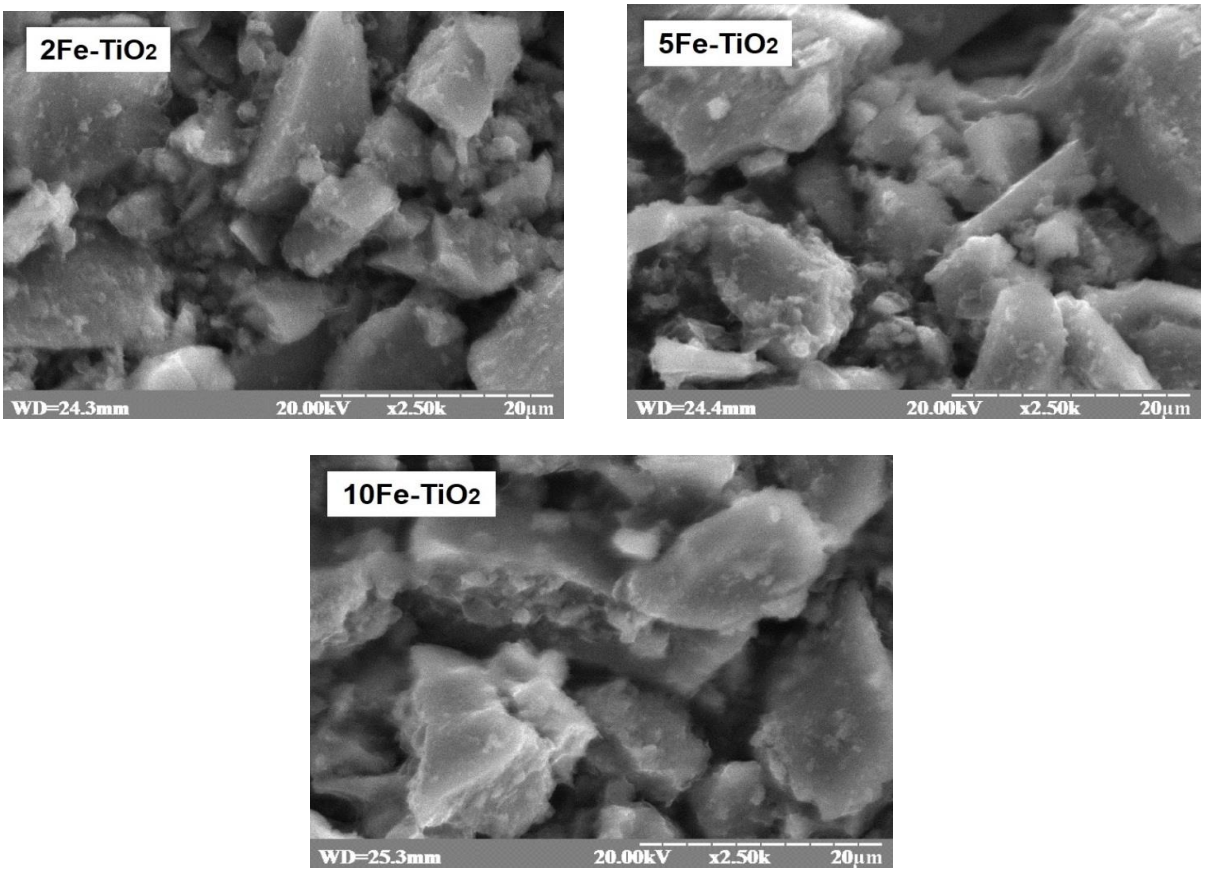

Fig. 4. Scanning electron micrographs of the Fe-doped TiO_2 sample.

2.2.4. Mossbauer spectroscopy

Room temperature Mössbauer spectra of all Fe-doped TiO_2 samples of only show symmetric doublets correspond to resonance absorption by the ^{57}Fe nucleus of tetrahedral coordinated Fe^{3+} ions in the high-spin state (Fig. 6). The close results were observed for Fe-doped anatase in [38] and [39]. All spectra were best fitted with two doublet components (D1 and D2) with different values of quadrupolar splitting (Qs(1) and Qs(2)) that can be explained by the localization of Fe^{3+} ions with the different surroundings symmetries located in the inner and outer layers of Fe-doped TiO_2 particles. It was observed that the changes of D1 and D2 components relative area ratio are within error that correspond to XRD data about close slight change in particle size with increase of iron concentration. In spherical particle approximation with outer and inner radius R_0 and R_{in} the ratio R_{in}/R_0 is in a range of 0.46-0.49. The calculations of Qs(1) values do not depend on the doping degree but simultaneous slightly increase Qs(2) values with the iron concentration in a range of 0.50-0.57 mm/s was observed (Table 3). Accordingly to [40] the measured value of quadrupolar splitting Q_S = 0.6 mm/s can be assigned to Fe^{3+} ions in solid solution in the anatase phase. The observed results are explained by gradual increase in distortion of the intracrystalline electric field with the doping degree growth.

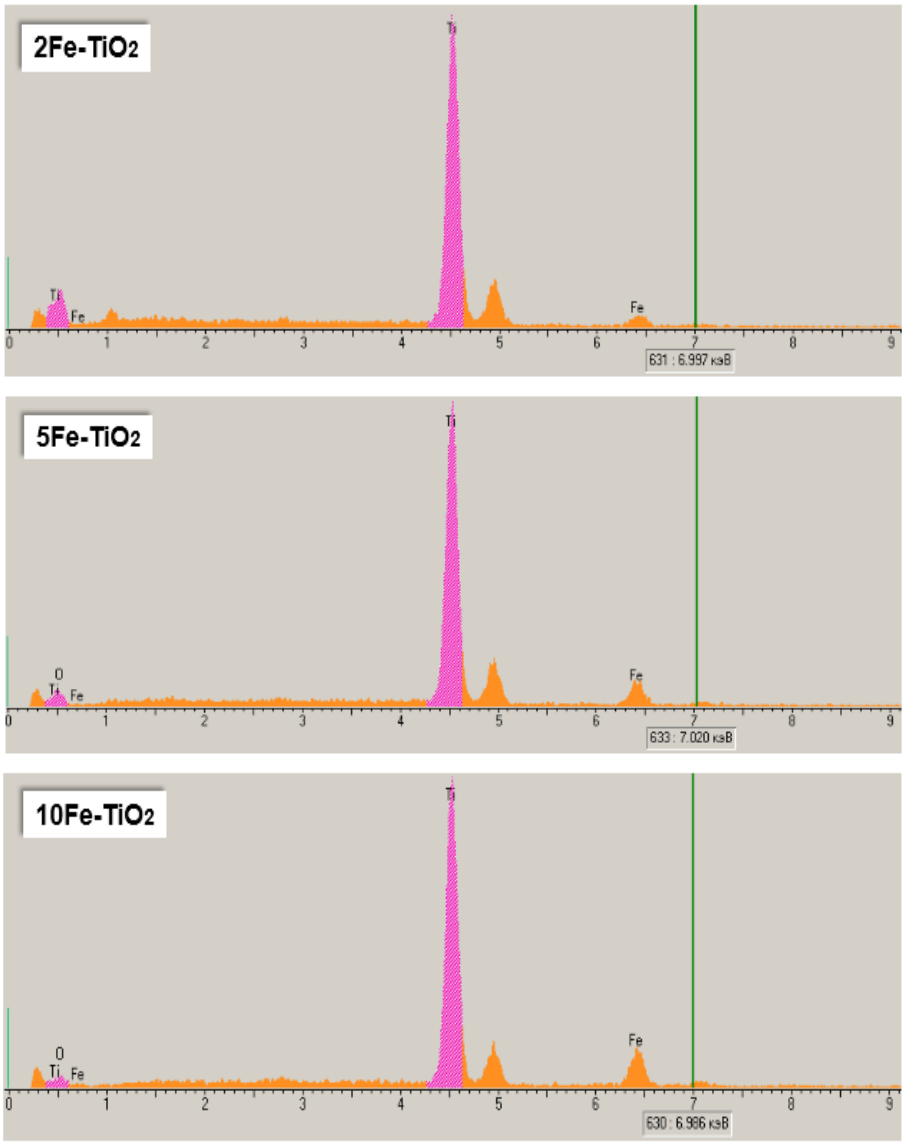

Element	wt.%
Ti	32.10
O	66.05
Fe	1.85
Total	100

Element	wt.%
Ti	30.85
O	65.40
Fe	3.75
Total	100

Element	wt.%
Ti	29.95
O	64.95
Fe	5.10
Total	100

Fig. 5. EDS spectra of the Fe-doped TiO_2 samples.

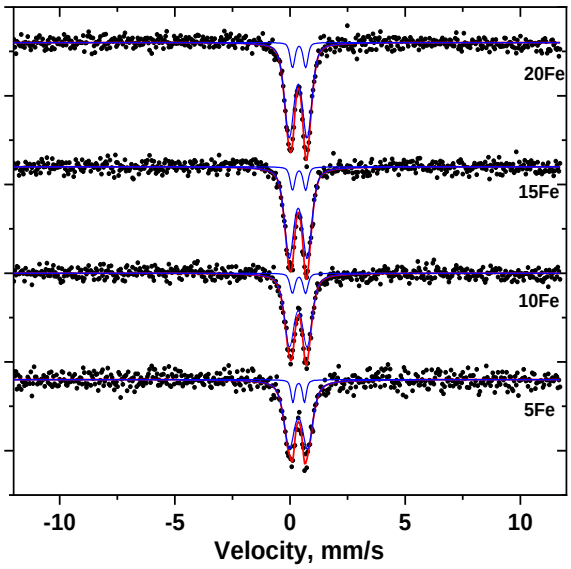

Fig. 6. Room-temperature Mössbauer spectra of the synthetized Fe-doped TiO_2

2.2.5. IR spectroscopy

Fig. 7 shows the IR spectra of raw titanium dioxide and Fe-doped TiO_2 samples, containing 2, 10 and 20 wt.% of Fe. The bands in the wavelength range 415-482 cm^{-1} and 537-604 cm^{-1} belong to the degenerate E_u oscillations of TiO_6 octahedra. The band in the wavelength range 475-482 cm^{-1} belongs to degenerate vibrations of anatase octahedra. The presence of bands with a maximum at 415-427 cm^{-1} on the spectra of 10Fe-TiO_2 and 20Fe-TiO_2 samples indicates the presence of structural rutile arrays in the anatase phase. The bands at 361 cm^{-1} and 722-745 cm^{-1} belong to symmetrical vibrations of A2u octahedra. In the spectra of samples with a high Fe content, there are bands with a maximum at 951-953 cm^{-1}. We attribute them to the valence vibrations of Ti-O-Fe bridges in oxide materials. The absorption band with a maximum at 1627-1635 cm^{-1} corresponds to the deformation vibrations of water molecules adsorbed on the oxide material surface. The shift of this band towards smaller wavelengths indicates a decrease in the adsorption energy between water molecules and surface of the iron-doped titania.

Table 3.

The parameters of the Mössbauer spectra of Fe-doped TiO_2 samples measured at 90 K (I_S is isomer shift; Q_S is quadrupole splitting; H is hyperfine field; S is relative integral intensity; G is line width)

	Site	I_S, mm/s	Qs, mm/s	S, %	G, mm/s
5Fe					
1	D1	0.365	0.79	89.4	0.55
2	D2	0.375	0.50	10.6	0.21
10Fe					
1	D1	0.358	0.77	88	0.52
2	D2	0.389	0.56	12	0.25
15Fe					
1	D1	0.355	0.78	88.7	0.49
2	D2	0.393	0.57	11.3	0.24
20Fe					
1	D1	0.355	0.78	88.4	0.49
2	D2	0.394	0.57	11.6	0.25

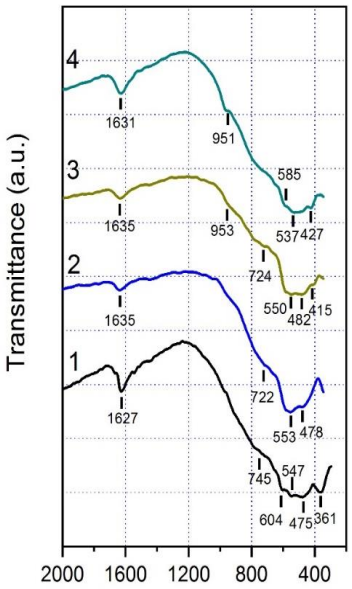

1 – a-TiO_2; 2 – 2Fe/TiO_2; 3 – 10Fe/TiO_2; 4 – 20Fe/TiO_2

Fig. 7. IR spectra of Fe-doped TiO_2 samples.

2.3. Photocatalytic studies

Evaluation of the photocatalytic activity of Fe-doped TiO_2 samples was investigated in degradation of the CR dye. The following factors influencing CR photodegradation were investigated: (i) the effect of Fe doping; (ii) the effect of hydrogen peroxide adding; and (iii) the effect of irradiation time. The CR concentration did not change in the absence of light. This means that CR adsorption do not take place on the samples surface. The photodestruction of CR dye did not occurs without photocatalysts. Thus, the presence of both photocatalyst and UV light have become necessary conditions for effective degradation of the CR dye.

2.3.1. Effect of Fe content

The effect of Fe content on the photocatalytic degradation of CR dye solution is demonstrated in Fig. 8a. The UV-Vis spectra of Congo Red solutions after photocatalysis onto Fe-doped TiO_2 samples are depicted in Fig. 8b. Fig. 8c demonstrates that the processes of CR dye degradation onto Fe-doped TiO_2 samples fitted well with the first-order kinetics model. The obtained values of the rate constant (k) (Table 4) demonstrate the overall dependence of CR photocatalytic degradation on Fe dopant content. The highest rate constant is 0.0437 min^{-1} for 2Fe-TiO_2 sample. Fig. 8d shows the degradation efficiency of Fe-doped TiO_2 samples. It can be seen that the photocatalytic activity 2Fe-TiO_2 sample is highest compared to other samples. The positive effect of Fe ions can be described by the efficient separation of photogenerated electrons and holes. Fe ions act as a trap for photogenerated carriers [35]:

$$TiO_2 + hv \rightarrow h^+ + e^- \quad (5)$$

$$Fe^{3+} + e^- \rightarrow Fe^{2+} \quad (6)$$

$$Fe^{2+} + O_{2\,abs} \rightarrow Fe^{3+} + O_2^- \quad (7)$$

$$Fe^{2+} + Ti^{4+} \rightarrow Fe^{3+} + Ti^{3+} \quad (8)$$

$$Fe^{3+} + hv_{vb}^+ \rightarrow Fe^{4+} \quad (9)$$

However, a further increase in the Fe ions content (5 wt.% and more) the photocatalytic efficiency of samples decreases. The reason is that Fe ions become recombination centers for electrons and holes [41]:

$$Fe^{3+} + e^- \rightarrow Fe^{2+} \quad (10)$$

$$Fe^{2+} + hv_{vb}^+ \rightarrow Fe^{3+} \quad (11)$$

$$Fe^{3+} + hv_{vb}^+ \rightarrow Fe^{4+} \quad (12)$$

$$Fe^{4+} + e^- \rightarrow Fe^{3+} \quad (13)$$

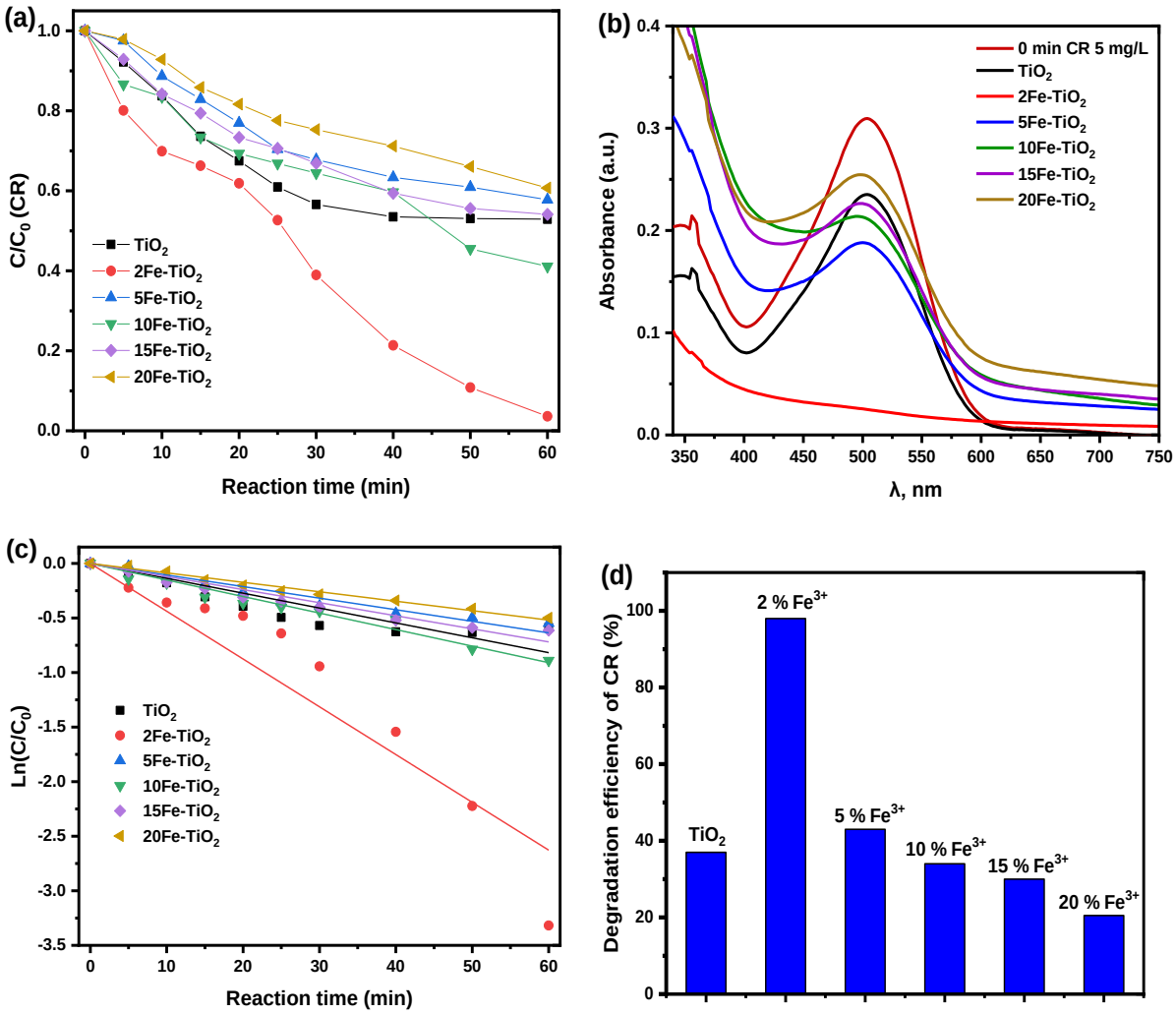

Fig. 8. (a) Effect of Fe content on the photocatalytic degradation of CR dye solution; (b) UV-vis spectra of Congo Red solutions after photocatalysis onto Fe-doped TiO_2 samples; (c) First-order kinetics model of CR degradation onto Fe-doped TiO_2 samples; (d) Degradation efficiency of Fe-doped TiO_2 samples (conditions: m(sample) = 30 mg, V(dye solution) = 20 mL; τ=60 min; C(CR)=5 mg/L; $C(H_2O_2)$=10 mM).

Table 4

The rate constant of the CR dye photodegradation reaction

Fe content (wt.%)	k (min^{-1})	R^2
0	0.0136	0.9301
2	0.0437	0.9461
5	0.0106	0.9768
10	0.0151	0.9886
15	0.0119	0.9811
20	0.0086	0.9936

These results suggest that the optimal Fe content is 2 wt.%. The sample 2Fe-TiO_2 possess the best photocatalytic activity and can degrade 98.1% of CR dye. The undoped TiO_2 sample demonstrate low photocatalytic activity: the CR dye degradation is only 37.2% within 1 hour under UV light. Thus, the 2Fe-TiO_2 sample contributes the lowest recombination of electron-hole pairs and thus demonstrates the highest photocatalytic properties. Comparison of the photocatalytic activity of different TiO_2-based materials towards different dyes is presented in Table 5.

Table 5

Comparison of photocatalytic activity of different TiO_2-based materials in dyes removal processes

Photocatalyst	Condition	Degradation extent, %	Ref.
7 % Fe^{3+}-doped TiO_2	Methylene blue (3 mg/L) under irradiation of visible light (4 h)	96.7	[34]
Fe^{3+}-doped TiO_2 with 0.05:1.00 M ratio of Fe and Ti	RhB (10 mg/L) solution at 40 °C operating temperature under 3.0 bar inlet pressure	91.1	[32]
0.3Fe-TiO_2	Malachite Green (5.0 mg/L), under irradiation of UV light (110 min)	85.0	[31]
5% Fe^{3+}-doped TiO_2	Methylene blue ($1.0*10^{-5}$M) under irradiation of UV light (8 h)	16.8	[42]
0.01% Fe–TiO_2/FAC	Methylene blue (20 mg/L) under irradiation of visible light	33.0	[22]
0.10% Fe–TiO_2	Methyl orange (30 mg/L), under irradiation of UV light (75 min)	79.0	[24]
GR/Fe-NWCs	Methylene blue (10 mg/L) under irradiation of UV light (1 h)	99.5	[23]
TiO_2-Fe_3O_4-bentonite	Methylene blue (30 mg/L) under irradiation of UV light (90 min)	90.0	[43]
Cu-loaded Fe_3O_4@TiO_2	Congo red (10 ppm) under irradiation of UV light (50 min)	71.7	[8]
2.5% N-TiO_2	Congo red (10 ppm) under irradiation of visible light (3 h), pH = 2.5	98.0	[7]
2% Fe^{3+}-doped TiO_2	Congo red (5 mg/L) under irradiation of UV light (30 min), H_2O_2 concentration 20 mM	99.4	This work

2.3.2. Effect of hydrogen peroxide

The effect of H_2O_2 and the determination of its optimal amount were investigated. It is known that hydrogen peroxide (H_2O_2) reacts with the electrons from the conduction band and the superoxide radicals, forming hydroxyl radicals (equations 14-15):

$$H_2O_2 + TiO_2(e_{CB}^-) \rightarrow OH^- + \cdot OH + TiO_2 \quad (14)$$

$$H_2O_2 + O_2^{\cdot -} \rightarrow OH^- + \cdot OH + O_2 \quad (15)$$

As a result, the addition of H_2O_2 accelerates the process of CR photocatalytic degradation. Fig. 9 shows the effect of H_2O_2 with different concentrations (5, 10, 15, and 20 mM) on the CR photocatalytic degradation. According to the obtained results, presented in Fig. 9a, H_2O_2 has a significant effect on CR degradation onto 2Fe-TiO_2 sample. The optimal concentration of H_2O_2 is 20 mM. Almost complete CR degradation was achieved in 30 minutes under UV light, while in the absence of H_2O_2 the photodegradation is only 33.9% after 1 hour. Moreover, in the absence of H_2O_2, the reaction rate constant is 0.0074, which is in 11.25 times lower than that obtained in the presence of 20 mM H_2O_2 onto 2Fe-TiO_2. It should be noted that in large quantities H_2O_2 acts as an absorber of holes and OH radicals (equations 16-18):

$$H_2O_2 + 2h_{VB}^+ \rightarrow O_2 + 2H^+ \quad (16)$$

$$H_2O_2 + \cdot OH \rightarrow H_2O + HO_2^{\cdot} \quad (17)$$

$$HO_2^{\cdot} + \cdot OH \rightarrow H_2O + O_2 \quad (18)$$

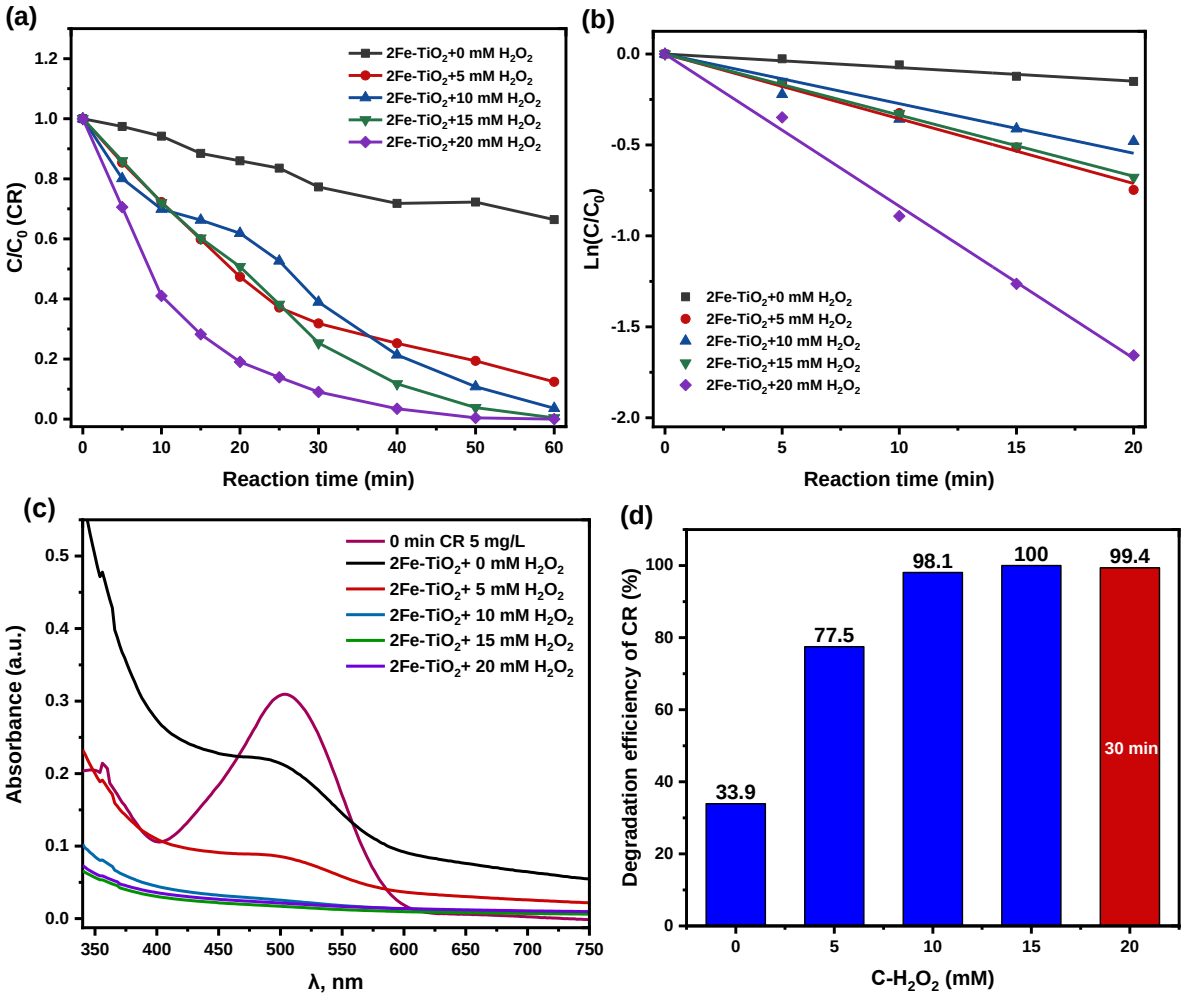

Fig. 9. Photocatalytic activity of 2Fe-TiO_2 sample: (a) Effect of H_2O_2 concentration on 20 mL of 5 mg/L CR degradation under UV light. Concentration of 2Fe-TiO_2 was 1.5 g/L. (b) First-order rate kinetics; (c) Conversion of CR (5 mg/L) as function concentrations of H_2O_2 under UV light in 60 min; (d) UV-Vis spectra of Congo Red solutions after UV irradiation for 60 min at indicated concentrations of CR and H_2O_2. The experimental conditions are the following: m(2Fe-TiO_2) = 30 mg, C(H_2O_2) = 0-20 mM.

Table 6

The parameters of the first-order kinetic model for the CR photodegradation in the presence of 2Fe-TiO_2 sample

C(H_2O_2)	k(min^{-1})	R^2
0 mM	0.0074	0.9892
5 mM	0.0355	0.9968
10 mM	0.0272	0.9673
15 mM	0.0336	0.9995
20 mM	0.0836	0.9984

2.3.3. Comparison of photocatalytic activities between 2Fe-TiO_2 and commercial Degussa P25-TiO_2

Commercial TiO_2 (P25, Degussa) is known as a highly efficient photocatalyst and is widely used as a model photocatalyst in dyes degradation studies [44]. Comparative studies between 2Fe-TiO_2 and P25-TiO_2 were performed in this study to evaluate the photocatalytic efficiency of the samples. Both photocatalysts achieved complete CR degradation within 30 minutes (Fig. 10) at a H_2O_2 concentration of 20 mM. The kinetic curves of CR degradation under UV light are presented in Fig. 10b. It can be concluded that the reactions belong to the first order kinetic model. Moreover, the rate constant *k* for P25-TiO_2 is 0.054 min^{-1}, which was only slightly higher than for 2Fe-TiO_2 (*k* = 0.083 min^{-1}) (Fig. 10b). Thus, 2Fe-TiO_2 demonstrate the same activity as P25-TiO_2 in the CR degradation under UV light.

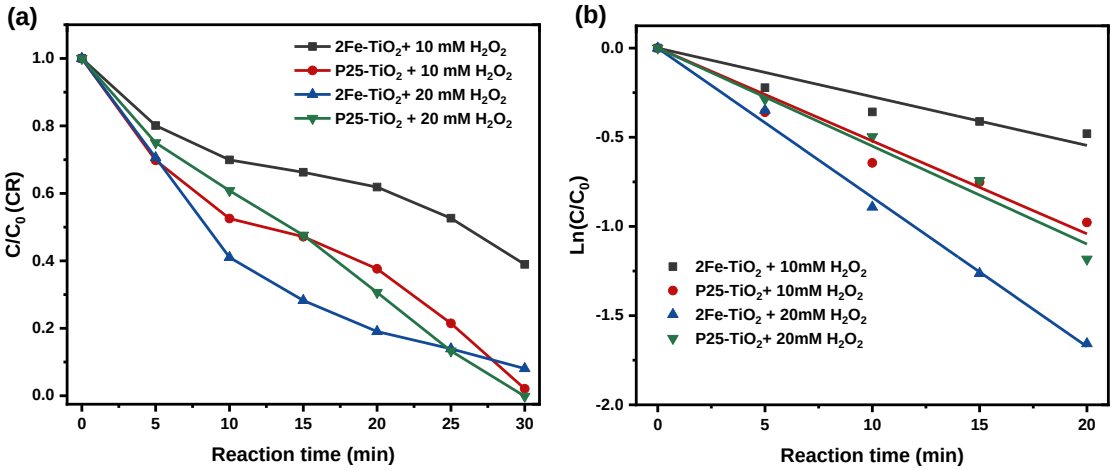

Fig. 10. Comparison of photocatalytic efficiencies of 2Fe-TiO_2 and P25-TiO_2 in the CR degradation under UV light and in the H_2O_2 presence: (a) The decolorizing of CR over time; (b) First-order rate kinetic model (conditions: C(CR) = 5 mg/L, photocatalyst dosage is 1.5 g/L).

Conclusion

Fe-doped TiO_2 photocatalysts were synthesized using a modified sol-gel method. The crystal structure of all samples is anatase. XRD analysis confirmed that the introduction of Fe ions causes structure amorphization. Fe-doped TiO_2 samples have mesoporous structure. The specific surface area of Fe-doped TiO_2 samples increases from 274 m^2g^{-1} (for 5Fe-TiO_2) to 416.4 m^2g^{-1} (for 20Fe-TiO_2). SEM and EDS analyses gave information about morphology and chemical composition of the samples. Mossbauer spectroscopy data confirm the presence of solid solution of Fe^{3+} ions in titania with the formation of Fe-doped TiO_2 particles which have a core-shell structure where the ratio between the radius of particle and its inner part is close to 0.5. IR spectroscopy confirmed the presence of anatase octahedra. Evaluation of the photocatalytic activity of Fe-doped TiO_2 samples was investigated in degradation of the CR dye. The processes of CR dye degradation onto Fe-doped TiO_2 samples fitted well with the first-order kinetics model. It was investigated that the photocatalytic activity 2Fe-TiO_2 sample is highest compared to other Fe-doped TiO_2 samples. The positive effect of Fe ions can be described by the efficient separation of photogenerated electrons and holes. The effect of H_2O_2 and the determination of its optimal amount were investigated. It was proved that the addition of H_2O_2 accelerates the process of CR photocatalytic degradation. The photocatalytic activity of the 2Fe-doped TiO_2 a slight higher than the efficiency of commercial TiO_2 (P25 Degussa). Comparison of this work with previous studies has shown that the photocatalyst 2Fe-TiO_2 is a very promising material for azo dyes degradation under UV-A light.

Acknowledgement

The authors thank the Ministry of Education and Science of Ukraine for financial support in the framework of project 0120U102035.

Ivan Mironyuk – Doctor of Chemical Sciences, Head of the Chemistry Department, Vasyl Stefanyk Precarpathian National University;
Nazarii Danyliuk – PhD student, leading specialist at the Educational and Scientific Center of Material Science and Nanotechnology, Vasyl Stefanyk Precarpathian National University;
Tetiana Tatarchuk – Associate Professor of the Chemistry Department, Director of Educational and Scientific Center of Material Science and Nanotechnology, Vasyl Stefanyk Precarpathian National University;
Ihor Mykytyn - Associate Professor of the Chemistry Department, Vasyl Stefanyk Precarpathian National University;
Volodymyr Kotsyubynsky - Doctor of Physical and Mathematical Sciences, Vasyl Stefanyk Precarpathian National University.

[1] K.T. Chung, Azo dyes and human health: A review, J. Environ. Sci. Heal. - Part C Environ. Carcinog. Ecotoxicol. Rev. 34, 233 (2016), https://doi.org/10.1080/10590501.2016.1236602 .
[2] A. Malik, E. Grohmann, Environmental protection strategies for sustainable development, 2012. https://doi.org/10.1007/978-94-007-1591-2.
[3] B. Lellis, C.Z. Fávaro-Polonio, J.A. Pamphile, J.C. Polonio, Effects of textile dyes on health and the environment and bioremediation potential of living organisms, Biotechnol. Res. Innov. 3, 275 (2019), https://doi.org/10.1016/j.biori.2019.09.001.

[4] F.M. Drumond Chequer, G.A.R. de Oliveira, E.R. Anastacio Ferraz, J. Carvalho, M.V. Boldrin Zanoni, D.P. de Oliveir, Textile Dyes: Dyeing Process and Environmental Impact, Eco-Friendly Text. Dye. Finish. (2013). https://doi.org/10.5772/53659.

[5] Z.A. AL-Othman, R. Ali, M. Naushad, Hexavalent chromium removal from aqueous medium by activated carbon prepared from peanut shell: Adsorption kinetics, equilibrium and thermodynamic studies, Chem. Eng. J. 184, 238 (2012), https://doi.org/10.1016/j.cej.2012.01.048.

[6] P.W. Wong, T.T. Teng, N.A.R. Nik Norulaini, Efficiency of the coagulation-flocculation method for the treatment of dye mixtures containing disperse and reactive dye, Water Qual. Res. J. Canada. 42, 54 (2007), https://doi.org/10.2166/wqrj.2007.008.

[7] H.S. Wahab, H.M. Hadi, Visible light N-TiO2-induced photodegradation of congo red: Characterization, kinetics and mechanistic study, Int. J. Environ. Sci. Technol. 14, 2135 (2017), https://doi.org/10.1007/s13762-017-1361-8.

[8] P. Arora, A. Fermah, J.K. Rajput, H. Singh, J. Badhan, Efficient solar light-driven degradation of Congo red with novel Cu-loaded Fe3O4@TiO2 nanoparticles, Environ. Sci. Pollut. Res. 24, 19546 (2017), https://doi.org/10.1007/s11356-017-9571-7.

[9] M. Movahedi, A.R. Mahjoub, S. Janitabar-Darzi, Photodegradation of Congo red in aqueous solution on ZnO as an alternative catalyst to TiO2, J. Iran. Chem. Soc. 6, 570 (2009), https://doi.org/10.1007/BF03246536.

[10] L. Nadjia, E. Abdelkader, B. Ahmed, Photodegradation study of Congo Red in Aqueous Solution using ZnO/ UV-A: Effect of pH And Band Gap of other Semiconductor Groups, J. Chem. Eng. Process Technol. 02, 1 (2011), https://doi.org/10.4172/2157-7048.1000108.

[11] C.A. Huerta-Aguilar, V. Palos-Barba, P. Thangarasu, R.T. Koodali, Visible light driven photo-degradation of Congo red by TiO2–ZnO/Ag: DFT approach on synergetic effect on band gap energy, Chemosphere. 213 (2018) 481–497. https://doi.org/10.1016/j.chemosphere.2018.09.053.

[12] N. Danyliuk, J. Tomaszewska, T. Tatarchuk, Halloysite nanotubes and halloysite-based composites for environmental and biomedical applications, J. Mol. Liq. 309 (2020). https://doi.org/10.1016/j.molliq.2020.113077.

[13] D. Ayodhya, G. Veerabhadram, A review on recent advances in photodegradation of dyes using doped and heterojunction based semiconductor metal sulfide nanostructures for environmental protection, Mater. Today Energy. 9. 83 (2018), https://doi.org/10.1016/j.mtener.2018.05.007.

[14] J. Singh, S. Kumar, Rishikesh, A.K. Manna, R.K. Soni, Fabrication of ZnO–TiO2 nanohybrids for rapid sunlight driven photodegradation of textile dyes and antibiotic residue molecules, Opt. Mater. (Amst). 107 (2020) 110138. https://doi.org/10.1016/j.optmat.2020.110138.

[15] R.K. Wahi, W.W. Yu, Y. Liu, M.L. Mejia, J.C. Falkner, W. Nolte, V.L. Colvin, Photodegradation of Congo Red catalyzed by nanosized TiO2, J. Mol. Catal. A Chem. 242, 48 (2005), https://doi.org/10.1016/j.molcata.2005.07.034.

[16] S. Province, Effect of pH on Adsorption and Photocatalytic Degradation Efficiency of Different Catalysts on Removal of Methylene Blue, Asian J. Chem. 26, 6097 (2014), https://doi.org/http://dx.doi.org/10.14233/ajchem.2014.17908.

[17] K. Aguilar, A. Garvín, A. Ibarz, Effect of the concentration on the kinetic model of the photo-degradation of 5-hydroxymethylfurfural by UV irradiation, J. Food Eng. 191, 67 (2016), https://doi.org/10.1016/j.jfoodeng.2016.06.026.

[18] N.A.M. Barakat, M.A. Kanjwal, I.S. Chronakis, H.Y. Kim, Influence of temperature on the photodegradation process using Ag-doped TiO2 nanostructures: Negative impact with the nanofibers, J. Mol. Catal. A Chem. 366, 333(2013), https://doi.org/10.1016/j.molcata.2012.10.012.

[19] M. Feilizadeh, F. Attar, N. Mahinpey, Hydrogen peroxide-assisted photocatalysis under solar light irradiation: Interpretation of interaction effects between an active photocatalyst and H2O2, Can. J. Chem. Eng. 97, 2009 (2019), https://doi.org/10.1002/cjce.23455.

[20] I. Ahmad, Q. Fasihullah, F.H.M. Vaid, Effect of light intensity and wavelengths on photodegradation reactions of riboflavin in aqueous solution, J. Photochem. Photobiol. B Biol. 82, 21 (2006), https://doi.org/10.1016/j.jphotobiol.2005.08.004.

[21] F.B. Li, X.Z. Li, The enhancement of photodegradation efficiency using Pt-TiO2 catalyst, Chemosphere. 48. 1103 (2002), https://doi.org/10.1016/S0045-6535(02)00201-1.
B. Wang, Q. Li, W. Wang, Y. Li, J. Zhai, Preparation and characterization of Fe 3+ -doped TiO 2 on fly ash cenospheres for photocatalytic application, Appl. Surf. Sci. 257, 3473 (2011), https://doi.org/10.1016/j.apsusc.2010.11.050.

[22] W. Li, X. Liu, H. Li, Hydrothermal synthesis of graphene/Fe3+-doped TiO2 nanowire composites with highly enhanced photocatalytic activity under visible light irradiation, J. Mater. Chem. A. 3, 15214 (2015), https://doi.org/10.1039/c5ta00763a.

[23] T. Tong, J. Zhang, B. Tian, F. Chen, D. He, Preparation of Fe3+-doped TiO2 catalysts by controlled hydrolysis of titanium alkoxide and study on their photocatalytic activity for methyl orange degradation, J. Hazard. Mater. 155, 572 (2008), https://doi.org/10.1016/j.jhazmat.2007.11.106.

[24] P. Pongwan, B. Inceesungvorn, K. Wetchakun, S. Phanichphant, N. Wetchakun, Highly efficient visible-light-induced photocatalytic activity of Fe-doped TiO 2 nanoparticles, Eng. J. 16, 143 (2012), https://doi.org/10.4186/ej.2012.16.3.143.
[25] I. Mironyuk, T. Tatarchuk, H. Vasylyeva, M. Naushad, I. Mykytyn, Adsorption of Sr(II) cations onto phosphated mesoporous titanium dioxide: Mechanism, isotherm and kinetics studies, J. Environ. Chem. Eng. 7 (2019) 103430. https://doi.org/10.1016/j.jece.2019.103430.
[26] I. Mironyuk, T. Tatarchuk, H. Vasylyeva, V.M. Gun'ko, I. Mykytyn, Effects of chemosorbed arsenate groups on the mesoporous titania morphology and enhanced adsorption properties towards Sr(II) cations, J. Mol. Liq. 282, 587 (2019), https://doi.org/10.1016/j.molliq.2019.03.026.
[27] I. Mironyuk, T. Tatarchuk, M. Naushad, H. Vasylyeva, I. Mykytyn, Highly efficient adsorption of strontium ions by carbonated mesoporous TiO 2, J. Mol. Liq. 285, 742 (2019), https://doi.org/10.1016/j.molliq.2019.04.111.
[28] K. Alamelu, B.M. Jaffar Ali, TiO2-Pt composite photocatalyst for photodegradation and chemical reduction of recalcitrant organic pollutants, J. Environ. Chem. Eng. 6 5720 (2018), https://doi.org/10.1016/j.jece.2018.08.042.
[29] D.I. Anwar, D. Mulyadi, Synthesis of Fe-TiO2 Composite as a Photocatalyst for Degradation of Methylene Blue, Procedia Chem. 17, 49 (2015), https://doi.org/10.1016/j.proche.2015.12.131.
[30] M. Asiltürk, F. Sayilkan, E. Arpaç, Effect of Fe3+ ion doping to TiO2 on the photocatalytic degradation of Malachite Green dye under UV and vis-irradiation, J. Photochem. Photobiol. A Chem. 203, 64 (2009), https://doi.org/10.1016/j.jphotochem.2008.12.021.
[31] G. Li, L. Yi, J. Wang, Y. Song, Hydrodynamic cavitation degradation of Rhodamine B assisted by Fe3+-doped TiO2: Mechanisms, geometric and operation parameters, Ultrason. Sonochem. 60 (2020) 104806. https://doi.org/10.1016/j.ultsonch.2019.104806.
[32] F. Han, V.S.R. Kambala, R. Dharmarajan, Y. Liu, R. Naidu, Photocatalytic degradation of azo dye acid orange 7 using different light sources over Fe3+-doped TiO2 nanocatalysts, Environ. Technol. Innov. 12, 27 (2018), https://doi.org/10.1016/j.eti.2018.07.004.
[33] D. Komaraiah, E. Radha, J. Sivakumar, M.V. Ramana Reddy, R. Sayanna, Structural, optical properties and photocatalytic activity of Fe3+ doped TiO2 thin films deposited by sol-gel spin coating, Surfaces and Interfaces. 17 (2019) 100368. https://doi.org/10.1016/j.surfin.2019.100368.
[34] H. Moradi, A. Eshaghi, S.R. Hosseini, K. Ghani, Fabrication of Fe-doped TiO2 nanoparticles and investigation of photocatalytic decolorization of reactive red 198 under visible light irradiation, Ultrason. Sonochem. 32, 314 (2016), https://doi.org/10.1016/j.ultsonch.2016.03.025.
[35] V.O. Kotsyubynsky, I.F. Myronyuk, L.I. Myronyuk, V.L. Chelyadyn, M.H. Mizilevska, A.B. Hrubiak, O.K. Tadeush, F.M. Nizamutdinov, The effect of pH on the nucleation of titania by hydrolysis of TiCl4: Der Einfluss des pH-Werts auf die Keimbildung von Titandioxid bei der Hydrolyse von TiCl4, Materwiss. Werksttech. 47 (2016) 288, https://doi.org/10.1002/mawe.201600491.
[36] N. Danyliuk, T. Tatarchuk, K. Kannan, A. Shyichuk, Optimization of TiO2-P25 photocatalyst dose and H2O2 concentration for advanced photo-oxidation using smartphone-based colorimetry, Water Sci. Technol. 84 469 (2021), https://doi.org/10.2166/wst.2021.236.
[37] C.E. Rodríguez-Torres, A.F. Cabrera, L.A. Errico, C. Adn, F.G. Requejo, M. Weissmann, S.J. Stewart, Local structure and magnetic behaviour of Fe-doped TiO2 anatase nanoparticles: Experiments and calculations, J. Phys. Condens. Matter. 20 (2008). https://doi.org/10.1088/0953-8984/20/13/135210.
[38] D. Cordischi, N. Burriesci, F. D'Alba, M. Petrera, G. Polizzotti, M. Schiavello, Structural characterization of Fe/Ti oxide photocatalysts by X-ray, ESR, and Mössbauer methods, J. Solid State Chem. 56, 182 (1985), https://doi.org/10.1016/0022-4596(85)90055-6.
[39] H.I. Masanori Hirano, Toyoko Joji, Michio Inagaki, Direct Formation of Iron(III)-Doped Titanium Oxide (Anatase) by Thermal Hydrolysis and Its Structural Property, J. Am. Ceram. Soc. 87, 35 (2008). https://doi.org/10.1111/j.1151-2916.2004.tb19941.x.
[40] W.C. Hung, Y.C. Chen, H. Chu, T.K. Tseng, Synthesis and characterization of TiO 2 and Fe/TiO 2 nanoparticles and their performance for photocatalytic degradation of 1,2-dichloroethane, Appl. Surf. Sci. 255 2205(2008). https://doi.org/10.1016/j.apsusc.2008.07.079.
[41] H.J. Lin, T.S. Yang, M.C. Wang, C.S. Hsi, Structural and photodegradation behaviors of Fe3+-doping TiO2 thin films prepared by a sol-gel spin coating, J. Alloys Compd. 610 478 (2014), https://doi.org/10.1016/j.jallcom.2014.05.053.
[42] W. Chen, H. Xiao, H. Xu, T. Ding, Y. Gu, Photodegradation of methylene blue by TiO2-Fe3O4-bentonite magnetic nanocomposite, Int. J. Photoenergy. 2015 (2015). https://doi.org/10.1155/2015/591428.
[43] T. Tatarchuk, N. Danyliuk, A. Shyichuk, W. Macyk, M. Naushad, Photocatalytic degradation of dyes using rutile TiO2 synthesized by reverse micelle and low temperature methods: real-time monitoring of the degradation kinetics, J. Mol. Liq. 342 (2021) 117407. https://doi.org/10.1016/j.molliq.2021.117407.

Іван Миронюк, Назарій Данилюк, Тетяна Татарчук, Ігор Микитин, Володимир Коцюбинський

Фотокаталітична деградація Конго Червоного в присутності Fe-допованого TiO_2

Прикарпатський національний університет імені Василя Стефаника, Івано-Франківськ, Україна, e-mail: danyliuk.nazariy@gmail.com

Fe-доповані TiO_2 (2, 5, 10, 15 і 20% мас. Fe) фотокаталізатори були синтезовані золь-гель методом з використанням титанового аквакомплексу у якості прекурсору. Структура та морфологія зразків охарактеризована Х-променевим та енергодисперсійним аналізом, інфрачервоною та мессбауерівською спектроскопією, скануючою електронною мікроскопією та методом BET. Х-променевий аналіз підтвердив утворення структури анатазу. Введення великої кількості іонів заліза в структуру титан(IV) оксиду викликає його аморфізацію. Розміри кристалітів отриманих зразків складають близько 3 нм. Синтезовані зразки TiO_2, леговані Fe, мають мезопористу структуру та високу питому площу поверхні (від 274 $м^2г^{-1}$ для 5Fe-TiO_2 до 416.4 $м^2г^{-1}$ для 20Fe-TiO_2). Дані мессбауерівської спектроскопії підтверджують вкорінення іонів Fe^{3+} до структури анатазу. Фотокаталітичну деградацію Конго червоного за допомогою фотокаталізаторів TiO_2, легованих Fe, досліджували під УФ-опроміненням. В результаті отримано оптимізовані умови для фотокаталітичної деградації Конго червоного у присутності пероксиду водню. Було виявлено, що зразок 2Fe-TiO_2 у присутності 20 мМ розчину H_2O_2 продемонстрував найбільшу ефективність при фотодеградації барвника (99.4%) під дією УФ-опромінення. Кінетику фотодеградації проаналізовано за допомогою смартфону та описано моделлю кінетики першого порядку.

Ключові слова: Fe-допований TiO_2; Фотокаталіз; Конго червоний; Смартфон.